HHS Public Access

Author manuscript

J Am Chem Soc. Author manuscript; available in PMC 2024 March 15.

Published in final edited form as:

J Am Chem Soc. 2023 March 15; 145(10): 5664–5673. doi:10.1021/jacs.2c10553.

Testing the Limits of Imbalanced CPET Reactivity: Mechanistic Crossover in H-atom Abstraction by Co(III)-oxo Complexes

Norman Zhao,

McKenna K. Goetz[†],

Joseph E. Schneider,

John S. Anderson[*]

Department of Chemistry, University of Chicago, Chicago, Illinois 60637, United States

Abstract

Transition metal-oxo complexes are key intermediates in a variety of oxidative transformations, notably C–H bond activation. The relative rate of C–H bond activation mediated by transition metal-oxo complexes is typically predicated on substrate bond dissociation free energy in cases with a concerted proton-electron transfer (CPET). However, recent work has demonstrated that alternative stepwise thermodynamic contributions such as acidity/basicity or redox potentials of the substrate/metal-oxo may dominate in some cases. In this context we have found basicity-governed concerted activation of C–H bonds with the terminal Co^{III}-oxo complex PhB($^{t\text{Bu}}$Im)Co^{III}O. We have been interested in testing the limits of such basicity-dependent reactivity and have synthesized an analogous, more basic complex, PhB($^{\text{Ad}}$Im)Co^{III}O, and studied its reactivity with H-atom donors. This complex displays a higher degree of imbalanced CPET reactivity than PhB($^{t\text{Bu}}$Im)Co^{III}O with C–H substrates and O–H activation of phenol substrates displays mechanistic crossover to stepwise PTET reactivity. Analysis of the thermodynamics of PT and ET reveal a distinct thermodynamic crossing point between concerted and stepwise reactivity. Furthermore, the relative rates of stepwise and concerted reactivity suggest that maximally imbalanced systems provide the fastest CPET rates up to the point of mechanistic crossover which results in slower product formation.

INTRODUCTION

Proton-coupled electron transfer (PCET), the transfer of a proton and an electron (equivalently a net hydrogen atom), and more specifically *concerted* proton-electron transfer (CPET, Scheme 1, purple diagonal) are fundamental elementary steps in synthetic and biological chemical reactions such as the activation and subsequent functionalization of kinetically inert C–H bonds by transition metal-oxo, imido, or nitrido complexes.[1–14] One prominent example in biology is Compound I, a high-valent Fe-oxo species formed in

[*]**Corresponding Author:** jsanderson@uchicago.edu.

[†]**Present Address:** Department of Chemistry, University of Wisconsin Madison 1101 University Avenue Madison WI 53706

Supporting Information.

Supplementary spectroscopic data and kinetic plots.

DFT-optimized XYZ coordinates of Co complexes and substrates.

cytochrome P450 enzymes that is responsible for the degradation of compounds such as pharmaceuticals via selective hydroxylation of unactivated aliphatic C–H bonds.[15–18] A number of synthetic transition metal-oxo model compounds have been isolated and studied in the context of C–H bond activation, yet harnessing these potent oxidants for controlled, selective reactivity remains an area of active research.[3,7,19–31]

The selectivity of transition metal-oxo complexes in CPET reactivity has traditionally been understood by comparing the BDFEs (bond dissociation free energies) of the substrate C–H bond being broken and the transition metal-hydroxide O–H bond being formed. The BDFE of a specific bond can be determined by using Equation 1,

$$\mathrm{BDFE} = 23.06\left(E^{0}\right) + 1.37(\mathrm{p}K_{a}) + C_{G}, \quad (1)$$

where pK_a is an acid dissociation constant for the given compound, E^0 is a one-electron reduction potential, and C_G is the standard reduction potential of $H^+/H^{\cdot}$ in a given solvent.[32,33] While these BDFE comparisons are founded on purely thermodynamic parameters, rates for concerted H-atom abstraction can be linked to the thermodynamics of net H-atom transfer, ΔG_{CPET}, by the Bell-Evans-Polanyi principle which holds that as a reaction becomes more exergonic, the activation barrier should become smaller leading to faster reactivity.[34–37] Indeed, several decades of study have demonstrated this trend dominates for H-atom abstraction by metal-oxo and related complexes.[37–39]

While concerted reactivity often dominates, particularly with C–H substrates, off-diagonal or stepwise processes with initial proton transfer (PT) or electron transfer (ET) must also be considered (Scheme 1, corner pathways). In fact, mechanistic crossover between concerted and stepwise reactivity has been observed in some cases.[40–55] Even in well-defined examples of CPET, the energies of stepwise PT or ET manifest through their net contribution to BDFEs and ΔG_{CPET} as seen in Equation 1.[23,33,40,56–60]

Although the idea that metal-oxo mediated C–H activation rates are dependent on ΔG_{CPET} has been the dominant mechanistic paradigm, recent experimental and computational results have suggested that the energetics of stepwise, or off-diagonal, intermediates can influence the rates of concerted reactions beyond their contributions to ΔG_{CPET}.[61] Srnec and coworkers introduced an asynchronicity parameter, η, to quantify the thermodynamic difference between driving forces for stepwise PT or ET.[40,62] A positive value of η corresponds to a CPET reaction with dominant PT character, while a negative value of η corresponds to a CPET reaction with dominant ET character. For similar overall ΔG_{CPET}, a greater magnitude ($|\eta|$) is expected to indicate a more imbalanced CPET transition state and a faster reaction. While such imbalanced transition states have been proposed in other reactions such as organic hydrogen transfer,[63] hydride transfer,[42] and pericyclic reactions,[64,65] there is significantly less support for such a phenomenon in metal-oxo mediated CPET reactions. Nevertheless, several groups, including our own, have recently observed CPET reactivity which displays a distinct dependence on the acidity and/or oxidation potential of substrates, despite having apparent concerted mechanisms.[40,43,56,66] These combined computational and experimental observations suggest that, in addition to limiting concerted or stepwise mechanisms, asynchronous or imbalanced pathways (Scheme

1, curved arrows) are viable, and perhaps common, in CPET reactivity. Indeed, there has been a vigorous debate in the literature around this possibility, particularly about how such trends would manifest in nonadiabatic systems with extensive proton tunneling.[56,59,67–73]

Our previous investigations of a terminal Co^{III}-oxo complex, $PhB(^{tBu}Im)_3Co^{III}O$, revealed rates of C–H activation that more strongly correlate with substrate pK_a rather than BDFE, consistent with an imbalanced CPET reaction in favor of basic (PT) reactivity.[40,57,59,66,74–76] Based on these results, we have been interested in synthesizing metal-oxo complexes with greater basicity to explore the frontier between imbalanced CPET reactivity and stepwise PTET reactivity. We recently reported an adamantyl (Ad) substituted Co^{III}-oxo complex, $PhB(^{Ad}Im)_3Co^{III}O$, which, given the greater electron donating properties of the Ad groups, is more basic than our previous Co^{III}-oxo complex.[77] Here we demonstrate that this enhanced basicity leads to more highly imbalanced CPET reactivity with C–H substrates. Exploration of activity with acidic phenol substrates reveals a switch from imbalanced CPET to stepwise reactivity featuring initial PT. Computational analysis of the thermodynamics of the reactivity with phenol substrates suggests that stepwise reactivity dominates when the energy to form stepwise intermediates becomes thermodynamically favorable. Interestingly, we observe that net PCET through stepwise PTET is significantly slower than CPET for substrates with BDFEs that differ by only ~1 kcal/mol. These results suggest that faster rates for H-atom abstraction can be realized with imbalanced transition states that take advantage of lower energy trajectories in the potential energy surface owing to more stable off-diagonal intermediates, but only up to the point where formation of these intermediates becomes favorable, leading to stepwise reactivity.

RESULTS AND DISCUSSION

C–H Activation Reactivity of $PhB(^{Ad}Im)_3Co^{III}O$

The synthesis and characterization of $PhB(^{tBu}Im)_3Co^{III}O$ (**1**^{tBu}) and $PhB(^{Ad}Im)_3Co^{III}O$ (**1**^{Ad}) have previously been reported by our group (Scheme 2).[57,76] A detailed mechanistic study of C–H activation reactivity was conducted for **1**^{tBu}, but a similar systematic study for **1**^{Ad} has not been performed. We have previously demonstrated that **1**^{Ad} is more basic and more reducing than **1**^{tBu}, as expected based on the more electron-donating Ad substituents on the imidazol-2-ylidene ligand scaffold.[77] Additionally, the BDFE of **3**^{Ad} is larger than that measured for **3**^{tBu}, providing additional driving force for H-atom abstraction. As **1**^{tBu} displays concerted C–H activation reactivity that predominantly trends with substrate pK_a (via imbalanced CPET), we hypothesized that the enhanced basicity of **1**^{Ad} would lead to more pronounced imbalanced CPET reactivity.

Initially we sought to reproduce the series of substrates screened with **1**^{tBu}. While **1**^{tBu} reacts with 9,10-dihydroanthracene (DHA, pK_a(DMSO) = 30) to form $PhB(^{tBu}Im)_3Co^{II}OH$ (**3**^{tBu}) and half an equivalent of anthracene in an isosbestic fashion, we were surprised to see that **1**^{Ad} did not perform the analogous reaction over several days. We thus investigated more acidic substrates that displayed faster reactivity with **1**^{tBu}. Indeed, **1**^{Ad} reacts cleanly with fluorene (pK_a(DMSO) = 18) to generate $PhB(^{Ad}Im)_3Co^{II}OH$ (**3**^{Ad}), albeit at a rate slower than **1**^{tBu}, contrary to what we would have predicted given the larger BDFE and pK_a

of $\mathbf{3^{Ad}}$ relative to $\mathbf{3^{tBu}}$. This is consistent with the increased steric bulk of the Ad groups playing a significant role in the C–H activation reactivity of $\mathbf{1^{Ad}}$. We therefore screened a variety of substrates with either secondary (2°) or tertiary (3°) reactive C–H bonds to account for steric differences between substrates that might affect reaction rates (Figure 1A, S1–6).

Not all of the thermodynamic parameters of interest (BDFE, oxidation potential, pK_a) have reliable literature values reported for all of the tested substrates, so we instead used DFT calculations to estimate the free energies of the CPET, PT1, and ET2 reactions between the metal-oxo and the substrate. We used an O3LYP/def2-SVP functional and basis set combination for these calculations and while it is likely that there are some systematic errors in the absolute values of these free energies, comparison between computed and experimental values shows a good correlation (Figure S7).[78–83] Furthermore, we note that the reactivity of $\mathbf{1^{tBu}}$, which was previously shown to correlate with experimental substrate pK_a, also shows a good correlation with computed ΔG_{PT1} (Figure 1A, $R^2 = 0.96$).

Screening several C–H substrates reveals a linear trend between ln(k_{obs})RT and ΔG_{PT1} for reaction with $\mathbf{1^{Ad}}$ (Figure 1A). Interestingly, we note that the trendlines for the 2° and 3° C–H substrates are parallel to each other, with similar slopes of ~0.4, within error. The identical slopes between the 2° and 3° demonstrates that steric effects don't influence the dependence on ΔG_{PT1}; the 3° phenylfluorene Hammett series should all be sterically very similar, and the same slope vs. ΔG_{PT1} in the 2° series suggests that sterics are not a major factor in the relative reactivity of this set either. However, the generally slower rates for the 3° substrates, manifested by the offset of this series from the data for the 2° series, suggests that the larger steric profile of the phenylfluorene substrates does impact reactivity relative to the 2° substrates. This steric influence is not observed for $\mathbf{1^{tBu}}$. These comparisons support that the observed trends with ΔG_{PT1} do not primarily arise from variations in proton tunneling distance, which has been invoked to explain imbalanced CPET reactivity in other systems.[69,71] Thus, despite this steric convolution in the Ad-system, the similar slopes observed for both substrate sets for $\mathbf{1^{Ad}}$ allow us to compare its dependence on ΔG_{PT1} with that of $\mathbf{1^{tBu}}$.

A comparison of the trendlines in the plots of ln(k_{obs})RT versus ΔG_{PT1} for $\mathbf{1^{tBu}}$ and $\mathbf{1^{Ad}}$ is consistent with more basic $\mathbf{1^{Ad}}$ exhibiting a larger rate dependence on ΔG_{PT1} than $\mathbf{1^{tBu}}$. Indeed, the slope observed for $\mathbf{1^{Ad}}$ is roughly double that of $\mathbf{1^{tBu}}$ (0.4 vs. 0.2). The observed slopes for $\mathbf{1^{Ad}}$ are quite large, supporting a large degree of PT transition state character. For contextualization, a value of 0.5 might be expected for a pure PT event.[56] Interestingly, extrapolation of the trendline for 2° substrates reacting with $\mathbf{1^{Ad}}$ suggests that the expected pseudo-first order rate constant for the reaction with DHA would be smaller than that for the self-decay of $\mathbf{1^{Ad}}$ (10^{-5}–10^{-6} s^{-1}). This suggests that, in addition to steric hindrance, the large ΔG_{PT1} dependency of $\mathbf{1^{Ad}}$ makes reactivity with weakly acidic C–H bonds sluggish.

We also performed a Hammett analysis to further understand the effects of the more donating Ad substituent on the character of the C–H activation transition state. In analogy with our previous study, we used a series of substituted 9-((4-X-phenyl)fluorenes. We note that the substrate scope of $\mathbf{1^{Ad}}$ is limited relative to $\mathbf{1^{tBu}}$ due to side reactions observed

with some substrates. In these cases, the UV-vis transformations are not isosbestic which we ascribe to organic radical products further reacting with $\mathbf{1}^{\mathbf{Ad}}$ or $\mathbf{3}^{\mathbf{Ad}}$ to form as-of-yet unidentified Co-containing products. Nevertheless, the Hammett slope determined for $\mathbf{1}^{\mathbf{Ad}}$ is positive and steeper than that of $\mathbf{1}^{t\mathbf{Bu}}$ (Figure 1B). This observation is consistent with a greater buildup of negative charge at the carbon atom of the C–H bond as would be expected for greater PT character in the transition state.[84,85] Finally, we note that comparison of rates with ΔG_{ET1} shows no clear correlation, consistent with PT driven reactivity (Figure S33).

These trends indicate that for a given substrate, $\mathbf{1}^{\mathbf{Ad}}$ lies further than $\mathbf{1}^{t\mathbf{Bu}}$ from a perfectly synchronous or balanced CPET diagonal in a thermodynamic square scheme and closer to a stepwise PTET pathway (Scheme 1). However, the enhanced steric profile of the Ad substituents generally mutes reactivity, mandating a narrower substrate scope for $\mathbf{1}^{\mathbf{Ad}}$. Given this, we turned to a series of 4-X-2,6-di(*tert*-butyl)phenols to provide a larger set of substrates with constant steric bulk around the reactive O–H bond to enable further exploration of the H-atom abstraction reactivity of $\mathbf{1}^{\mathbf{Ad}}$. Additionally, these substrates comprise a set of more acidic H-atom donors, allowing us to test the limits of imbalanced CPET.

H-atom Abstraction from Phenols: Mechanistic Crossover to Stepwise Reactivity

While O–H bonds differ from C–H bonds due to their polarity, we reasoned that this isosteric series of phenols would allow us to examine a greater number of viable substrates with a pK_a range spanning 11 units (7.3–18.2, Table S3).[86,87] Furthermore, we were interested in seeing if the enhanced acidity of phenol substrates led to even more imbalanced reactivity or other emergent trends.

Complex $\mathbf{1}^{\mathbf{Ad}}$ exhibits clean reactivity with 10 equivalents of a subset of 4-X-2,6-di(*tert*-butyl)phenols (pK_a(DMSO) = 17.3–18.2) at −100 °C to form $\mathbf{3}^{\mathbf{Ad}}$ over ~5 minutes (Figures S9–S12). A representative reaction with 2,4,6-(^{t}Bu)$_3$-C$_6$H$_2$OH in THF is shown in Figure 2A. We measure a small deuterium KIE of 1.1(3) for this substrate, although it is difficult to interpret this value without more detailed variable temperature KIE measurements. During these studies, however, we noted distinct reactivity with some substrates, particularly those with enhanced acidity. For instance, $\mathbf{1}^{\mathbf{Ad}}$ reacts with 10 equivalents of 4-CO$_2$Me-2,6-(^{t}Bu)$_2$C$_6$H$_2$OH (pK_a(DMSO) = 11.9) at −100 °C to form a new green intermediate which can be assigned as [PhB(^{Ad}Im)$_3$Co^{III}OH]$^+$ ($\mathbf{2}^{\mathbf{Ad}}$) based on comparison to independently prepared samples (Figure 2B).[77] This suggests that, unlike C–H substrates and less acidic phenols, $\mathbf{1}^{\mathbf{Ad}}$ reacts initially via PT with this substrate at low temperature. The subsequent electron transfer is observed only upon warming to 0 °C, resulting in the formation of $\mathbf{3}^{\mathbf{Ad}}$ (Figure 2C), indicating a slower net rate of product formation. We note that we are not able to observe the final organic phenoxy radical presumably formed upon net H-atom transfer, although this is perhaps unsurprising as similar phenoxy radicals have been reported to undergo dimerization in solution.[48] Gas Chromatography/Mass Spectrometry analysis of the reaction mixtures supports the formation of dimerized phenoxy radicals for the 4-H and 4-NO$_2$ substituted phenols (Figures S34 and S35). The clear suggestion from these studies is that a substrate dependent mechanistic switch is observed for more acidic phenols.

Kinetic Trends with Thermodynamic Parameters

This clear mechanistic switch prompted us to examine trends between ln(k_{obs})RT calculated for phenol O–H activation and various thermodynamic parameters, akin to our analysis with C–H substrates above (Table 1). As with the C–H substrates, not all of the parameters of interest (oxidation potential and pK_a) have reliable literature values reported for all of the tested substrates and thus we again used DFT calculations to estimate the free energies of CPET, PT1, and ET2. As above, comparison between computed and experimental values shows a good correlation (Figures S23–25).

Initial comparison between the rate constants (adjusted for the temperature of reaction) and the free energies of net H-atom transfer, ΔG_{CPET}, shows no clear correlation (Figure 3A). While a general trend of smaller ln(k_{obs})RT values for less exergonic reactions is observed for the substrates that display concerted reactivity, as is typical for phenol substrates, the linear fit has an extremely shallow slope of ~0.03. Similarly unconvincing trends are observed with the asynchronicity parameter, η (a measure of the imbalanced nature of the transition state, Figure S28), despite clear correlations being observed previously for the C–H activation reactivity of **1**^{tBu}.[57] The substrates that are observed to follow a stepwise PT pathway also do not display any easily interpretable correlation with ΔG_{CPET} or η, however they do give a better linear correlation with ΔG_{PT1}, as expected (Figure 3B). Still, we note an anomalously small slope of 0.01 even with this expected trend. In contrast, the CPET substrates do not display any interpretable correlation with ΔG_{PT1}. The origin of the unclear and shallow correlations in these data is not immediately apparent. It is possible that cross-correlations between the energetics of CPET and PT, significant tunneling effects as we have observed with C–H substrates, hydrogen bonding effects, or some combination of these factors convolute reactivity trends.[88] Despite the complicated trends between the observed kinetics and computed thermodynamic parameters, there are several key conclusions that can be drawn from this data.

Firstly, the correlation between $k_{obs,PT}$ for the stepwise substrates and ΔG_{PT1} can be used to assess the possible agency of similar stepwise PTET mechanisms for the apparently concerted substrates. Extrapolation of this trend to the ΔG_{PT1} values for the concerted substrates provides a “ceiling” for the maximum expected $k_{obs,PT}$ for such a process (see SI). While some substrates lie near or below this line, the OMe substituted phenol is clearly above this line, demonstrating that for this substrate, and likely all the concerted substrates, a stepwise mechanism is not viable. This clearly supports the agency of a concerted mechanism in these reactions, a conclusion which is supported by data for the rates of ET reactivity with the stepwise phenols (see below).

The second conclusion is a thermodynamic “crossover” point between stepwise and concerted substrates. While plots of ln(k_{obs})RT vs. ΔG_{CPET} and η do not have a clear delineation between these mechanistic regimes, the plot of ln(k_{obs})RT vs. ΔG_{PT1} shows a break at ~+2 kcal/mol. As mentioned above, while the relative trend with ΔG_{PT} is reliable, it is likely that there is some systematic error in the DFT-computed values of ΔG_{PT1}. Thus, this break point can be crudely approximated as thermoneutral. This observation is somewhat intuitive: substrates which adopt a stepwise mechanism are those for which

the PT1 intermediate is thermodynamically favorable. This also serves as a simple metric for determining whether a given PCET reaction will likely proceed through a stepwise or concerted mechanism in this system. A roughly thermoneutral breakpoint between concerted and stepwise reactivity has also been proposed for basic Mn-oxo complexes and oxidizing Cr-oxo complexes.[89,90]

The last major conclusion relies upon comparing the overall stepwise versus concerted rates. The stepwise nature with some substrates provides the ability to investigate the relative rates of the fundamental PT1, ET2, and unified CPET steps in more detail. Specifically, we were interested in comparing rate-limiting $k_{obs,ET}$ of the stepwise process to $k_{obs,CPET}$ of the concerted phenol substrates. We measured the pseudo-first order rate constant for the reaction between independently prepared **2^{Ad}** and 10 equivalents of [TBA][4-CO_2Me-2,6-(^{t}Bu)$_2$C$_6$H$_2$O] (TBA = tetrabutylammonium) at varying temperatures (Figures S16–S18 and Table S4). An Arrhenius fit suggests that $k_{obs,ET}$ at −100 °C is very small, ~10^{-8} s^{-1} (Figure S19). Importantly, this rate constant is many orders of magnitude smaller than any of the $k_{obs,CPET}$ values measured for the concerted phenol substrates at the same temperature (see below, Table 1). We have also analyzed the reaction of **2^{Ad}** with 10 equivalents of [TBA][4-Br-2,6-(^{t}Bu)$_2$C$_6$H$_2$O] (Figure S20, Table S4). While this data quality is somewhat poorer, we can estimate a rate constant of ~10^{-3} s^{-1} for this ET reaction at −100 °C, which is also significantly smaller than $k_{obs,CPET}$ for any of the concerted substrates. This suggests that stepwise mechanisms are overall slower than concerted reactions with similar driving forces for net H-atom transfer. This likely arises from a slow ET step which implies a large reorganization energy. Such a large reorganization energy might be expected for a change from low-spin Co(III) to high-spin Co(II), and DFT calculations support this hypothesis with an estimated energy of 43 kcal/mol (Table S6). As a final note, the relative trend in ET rates further excludes stepwise PTET reactivity for the concerted substrates. Using extrapolated PT and ET rates from the stepwise reactions suggests that a PTET mechanism should be several orders of magnitude slower than the observed rates for the concerted phenols (see Table S5).

The slow observed ET rates allow for an illustrative comparison between 4-Br-2,6-(^{t}Bu)$_2$C$_6$H$_2$OH and 2,6-(^{t}Bu)$_2$C$_6$H$_2$OH. These two substrates have very similar (within ~1 kcal/mol) driving forces for CPET as well as asynchronicity values (Table 1). Despite this similarity, the $k_{obs,CPET}$ or $k_{obs,ET}$ rates for net H-atom transfer are very different between the two substrates, roughly an order of magnitude slower for the Br-substituted phenol. This observation is noteworthy as, despite a slightly smaller computed driving force, the concerted substrate reacts significantly faster. Thus, in thinking of design parameters for rapid H-atom abstraction, concerted reactivity seems to be beneficial.[52] Furthermore, systems with imbalanced thermodynamic driving forces should realize their fastest net H-atom transfer rates up until the point where stepwise PT or ET reactivity becomes thermodynamically favorable. At this point, a crossover to stepwise reactivity may be expected to slow rates as the system becomes trapped in an intermediate state.

This conclusion is somewhat different than observations for other PCET systems with concerted or stepwise reactivity, particularly in multi-site electrochemical or photochemically driven systems.[71] In these systems, mechanistic crossover to stepwise

reactivity is also observed for larger driving forces of separate proton transfer and electron transfer (i.e. smaller ΔG_{PT1} or ΔG_{ET2}). However, this stepwise reactivity is noted to be faster, not slower, than a concerted mechanism. One key difference to note between these examples and our system is that in synthetic complexes, such as $\mathbf{1^{Ad}}$, variations in PT energetics are typically compensated by similar and counteracting changes in ET energetics. This leads to the overall driving forces for net CPET being relatively constant, i.e. a lower ΔG_{PT1} typically correlates to less negative ΔG_{PT2}, and therefore a similar ΔG_{CPET}. For comparison, in multi-site PCET systems with electrochemical, and in some cases photochemical, driving forces, changing the base does not affect the thermodynamics of ET, and instead the overall driving force changes, i.e. A lower ΔG_{PT1} has no bearing on ΔG_{ET2} and therefore directly impacts ΔG_{CPET}. This prevents the stepwise intermediates from becoming a thermodynamic well. Thus, these different approaches probe the effect of thermodynamic parameters in different contexts. Regardless, all of these systems provide useful information for how different thermodynamic parameters can influence PCET reactivity, and further studies will be required for a holistic model in this evolving area.

CONCLUSION

We have investigated the H-atom abstraction reactivity of a highly basic Co-oxo complex. Reactivity with C–H substrates is consistent with prior findings of imbalanced or asynchronous CPET reactivity, with a more pronounced effect of ΔG_{PT1} attributed to the enhanced basicity of this oxo complex. Investigation of more acidic phenol substrates reveals a mechanistic crossover from CPET to stepwise PTET reactivity. Such mechanistic crossover is rare in molecular PCET reactions and provides the opportunity to investigate how the individual PT, ET, and CPET thermodynamics govern reaction pathways.

An analysis of these thermodynamics reveals that the determining factor governing mechanistic crossover in this case is ΔG_{PT1}, where a mechanistic switch occurs when PT1 becomes thermodynamically favorable. Furthermore, kinetic analysis of the individual PT1 and ET2 steps verifies a concerted mechanism for the apparently concerted substrates and goes further to suggest that concerted mechanisms have faster overall rates than stepwise mechanisms for similar driving forces. These findings suggest an optimal thermodynamic paradigm for fast H-atom transfer reactivity, at least for imbalanced or asynchronous systems. Imbalanced reactions will be accelerated as the thermodynamics of stepwise intermediates become increasingly favorable. However, this gain in rate only occurs up to the point where the formation of stepwise intermediates becomes exergonic. At this point, stepwise mechanisms can occur and trap the system in an intermediate state, which slows down net PCET reactivity. This emergent mechanistic picture has implications for the design of more rapid and selective PCET reactions, namely suggesting that the fastest rates will be realized with low-lying stepwise intermediates, as long as the formation of those stepwise intermediates is not energetically downhill.

EXPERIMENTAL SECTION

Materials and Instrumentation

All manipulations were performed under a dry nitrogen atmosphere using either standard Schlenk techniques or in an mBraun Unilab Pro glove box unless otherwise stated. All chemicals were obtained from commercial sources and used as received unless otherwise stated. Solvents were dried on a solvent purification system from Pure Process Technologies and passed through a column of activated alumina before storing over 4 Å molecular sieves under N2. Diethyl ether and tetrahydrofuran (THF) were stirred over NaK alloy and passed through a column of activated alumina prior to storing over 4 Å sieves under N_2. The substituted phenylfluorenes, and 3-phenylindene as well as compounds **1**-**3** were prepared according to literature procedures.[57,91] $HNEt_3BF_4$ was synthesized by stirring equimolar HBF_4•Et_2O and NEt_3 (500 mg) in Et_2O for 1 h. The reaction mixture was then concentrated *in vacuo* and the product was obtained as a white solid. Tetrabutylammonium phenolate salts were generated by adding tetrabutylammonium hydroxide (in methanol) to a solution of the substituted phenol (2 mmol) in benzene. The corresponding phenolate salt was then concentrated *in vacuo* and isolated. ^{1}H NMR of these reaction mixtures confirms consumption of the starting material through disappearance of the phenolic proton peak. UV-vis spectra were recorded on a Thermo Scientific Evolution 300 spectrometer with the VISIONpro software suite. A standard 1 cm quartz cuvette with an air-tight screw cap equipped with a puncturable septum was used for all measurements. A Unisoku CoolSpek cryostat was used for low temperature measurements. All kinetic traces were fit to the following equation: $A_t = A_{inf} + (A_0 - A_{inf})*\exp(-kt)$, where A_t is absorbance at time t, A_{inf} is the absorbance of the products at infinite time, A_0 is the initial absorbance of the reactants, k is the rate constant, and t is time in seconds. Errors are reported as the standard errors of the mean, except for k_{ET2} extrapolations for stepwise substituted phenols, which are reported as standard errors. ^{1}H NMR spectra were recorded using either Bruker DRX-400 or AVANCE-500 spectrometers and referenced to residual solvent peaks. Gas chromatography/mass spectrometry (GC/MS) data were collected on an Agilent SQ GC/MS with 5977A single quad MS and 7890B GC.

Density Functional Theory (DFT) Calculations

DFT calculations for the ground state energies of the C–H and O–H substrates were performed using the def2/SVP basis set and O3LYP functional on all atoms.[82,83] For calculations of the ground state energies of compounds **1–3**, the def2/SVP basis set and O3LYP functional was used except for Co, O, N and carbene C's where def2/TZVVP was used. All computations were carried out with the RIJCOSX approximation and a COSMO THF solvent correction with the ORCA program package (version 4.2.0).[92,93] Numerical frequency calculations were performed verify the optimized geometries were true minima and to obtain the free energies of all compounds. The Gibbs free enthalpy was used for all G values, defined as the total enthalpy (zero-point, electronic, vibrational, rotational, and translational components) less the total entropy correction (electronic, vibrational, rotational, and translational components). As defined in Scheme 2, ΔG_{CPET}, ΔG_{PT1}, ΔG_{ET2} and η values were calculated using the following equations:

$$\Delta G_{\mathrm{CPET}} = G_{\mathrm{M-OH}} + G_{\mathrm{C}}\cdot - G_{\mathrm{M=O}} - G_{\mathrm{C-H}}, \quad (2)$$

$$\Delta G_{\mathrm{PT1}} = G_{\mathrm{M-OH+}} + G_{\mathrm{C:-}} - G_{\mathrm{M=O}} - G_{\mathrm{C-H}}, \quad (3)$$

$$\Delta G_{\mathrm{ET2}} = G_{\mathrm{M-O-}} + G_{\mathrm{C-H+}} - G_{\mathrm{M=O}} - G_{\mathrm{C-H}}, \quad (4)$$

$$\eta = G_{\mathrm{M-OH+}} + G_{\mathrm{C:-}} - G_{\mathrm{M-O-}} - G_{\mathrm{C-H+}}\cdot, \quad (5)$$

where $G_{\mathrm{M=O}}$ is the calculated free energy of the Co-oxo complex, and $G_{\mathrm{C-H}}$ is the calculated free energy of the substrate.[62] All other free energies are defined analogously.

Kinetic Measurement Procedures

General Experimental Procedure for C–H Substrate Kinetics—To a screw-top cuvette equipped with a stirbar was added 2.0 mL of a 1.25 mM solution of $\mathbf{1^{Ad}}$ in THF in the glovebox. The cuvette was sealed and brought out of the glovebox. The cuvette was then transferred to a Unisoku cryostat, with positive Ar gas flow. At room temperature, 50 equiv. substrate dissolved in THF (100 μL) was injected through the septum, and the reaction was monitored by UV-vis spectroscopy (with stirring) for approximately 3 half-lives. Single wavelength monitoring at 720 nm was used for 3-phenylindene (0.5 s intervals). Full wavelength (300–1100 nm) monitoring was used for fluorene (3 min intervals). For indene, the region between 300 and 800 nm was scanned (30 s intervals). The absorbance data at 470 nm were used to generate the fit to the kinetic data to determine the observed rate constant. Three trials were carried out for each substrate and the rate constants averaged.

General Experimental Procedure for O–H Substrate CPET and PT Kinetics—To a screw-top cuvette equipped with a stirbar was added 2.0 mL of a 1.25 mM solution of $\mathbf{1^{Ad}}$ in THF in the glovebox. The cuvette was sealed and brought out of the glovebox. The cuvette was then transferred to a Unisoku cryostat, with positive Ar gas flow. The cryostat was cooled to −100 °C, and 10 equiv. 4-X-2,6-di(*tert*-butyl)phenol substrate (X = H, Me, OMe, ^{t}Bu, CO_2Me, Br, NO_2) dissolved in THF (100 μL) was injected through the septum, and the reaction was monitored by UV-vis spectroscopy (with stirring) at 720 nm for three half-lives with data recorded (1 second intervals). The absorbance data at 720 nm were used to generate the fit to the kinetic data to determine the observed rate constant. Three trials were carried out for each substrate and the rate constants averaged.

General Experimental Procedure for O–H Substrate ET Kinetics—To a screw-top cuvette equipped with a stirbar was added 2.0 mL of a 1.25 mM solution of $\mathbf{1^{Ad}}$ in THF in the glovebox. The cuvette was sealed and brought out of the glovebox. The cuvette was then transferred to a Unisoku cryostat, with positive Ar gas flow. The cryostat was cooled to −100 °C, then 1.5 equiv. $HNEt_3BF_4$ as a solution in MeCN (100 μL) was injected through the septum, and the reaction to form $\mathbf{2^{Ad}}$ was monitored by UV-vis spectroscopy. After 5 minutes, the cryostat was set to the temperature of interest (T = 0 °C, 5 °C, and 10 °C for X = CO_2Me; T = −90 °C, −85 °C and −80°C for X = Br) and allowed to

equilibrate for 15 minutes before 10 equiv. of TBA 4-X-2,6-di-tertbutylphenolate was added as a solution in THF (X = Br, CO_2Me). The reaction was monitored by UV-vis spectroscopy (with stirring) at 720 nm for approximately 3 half-lives (1, 5 or 20 second intervals). The absorbance data at 720 nm were used to generate the fit to the kinetic data to determine the observed rate constant. Three trials were carried out at 5 °C for X = CO_2Me, while the other substrate/temperature conditions were run once. The average rate constant obtained at 5 °C for X = CO_2Me was assumed to be representative of the error at other temperatures for that substrate. The variable temperature data were subsequently fit using the Arrhenius equation to determine the expected rate constants at −100 °C.

Supplementary Material

Refer to Web version on PubMed Central for supplementary material.

ACKNOWLEDGMENT

Work presented here was funded by the following sources: the National Institutes of Health through award R35 GM133470, an NSF CAREER award Grant No. 1654144, and the University of Chicago. N.Z. was primarily funded by the National Science Foundation Graduate Research Fellowship under Grant No. DGE-1746045. J.E.S. thanks the Department of Defense for a National Defense Science and Engineering Graduate Fellowship (00003765), and J.S.A. thanks the Sloan Foundation for a Research Fellowship (FG-2019-11497), the Dreyfus Foundation for a Teacher-Scholar Award (TC-21-064), and the 3M Corporation for an NTFA. The authors are grateful for the support of the University of Chicago Research Computing Center for assistance with the calculations carried out in this work. This paper is adapted from a thesis.

REFERENCES

(1). Larson VA; Battistella B; Ray K; Lehnert N; Nam W Iron and Manganese Oxo Complexes, Oxo Wall and Beyond. Nat. Rev. Chem 2020, 4, 404–419.

(2). Borovik AS Role of Metal–Oxo Complexes in the Cleavage of C–H Bonds. Chem. Soc. Rev 2011, 40, 1870–1874. [PubMed: 21365079]

(3). Murray PRD; Cox JH; Chiappini ND; Roos CB; McLoughlin EA; Hejna BG; Nguyen ST; Ripberger HH; Ganley JM; Tsui E; Shin NY; Koronkiewicz B; Qiu G; Knowles RR Photochemical and Electrochemical Applications of Proton-Coupled Electron Transfer in Organic Synthesis. Chem. Rev 2022, 122, 2017–2291. [PubMed: 34813277]

(4). Fukuzumi S; Cho K-B; Lee Y-M; Hong S; Nam W Mechanistic Dichotomies in Redox Reactions of Mononuclear Metal–Oxygen Intermediates. Chem. Soc. Rev 2020, 49, 8988–9027. [PubMed: 33316016]

(5). Bullock RM; Chen JG; Gagliardi L; Chirik PJ; Farha OK; Hendon CH; Jones CW; Keith JA; Klosin J; Minteer SD; Morris RH; Radosevich AT; Rauchfuss TB; Strotman NA; Vojvodic A; Ward TR; Yang JY; Surendranath Y Using Nature's Blueprint to Expand Catalysis with Earth-Abundant Metals. Science 2020, 369, eabc3183. [PubMed: 32792370]

(6). Wang F; Stahl SS Electrochemical Oxidation of Organic Molecules at Lower Overpotential: Accessing Broader Functional Group Compatibility with Electron–Proton Transfer Mediators. Acc. Chem. Res 2020, 53, 561–574. [PubMed: 32049487]

(7). Gentry EC; Knowles RR Synthetic Applications of Proton-Coupled Electron Transfer. Acc. Chem. Res 2016, 49, 1546–1556. [PubMed: 27472068]

(8). Kojima T Development of Functionality of Metal Complexes Based on Proton-Coupled Electron Transfer. Dalton Trans. 2020, 49, 7284–7293. [PubMed: 32309831]

(9). Nocera DG Proton-Coupled Electron Transfer: The Engine of Energy Conversion and Storage. J. Am. Chem. Soc 2022, 144, 1069–1081. [PubMed: 35023740]

(10). Lee JL; Ross DL; Barman SK; Ziller JW; Borovik AS C–H Bond Cleavage by Bioinspired Nonheme Metal Complexes. Inorg. Chem 2021, 60, 13759–13783. [PubMed: 34491738]

(11). Pannwitz A; Wenger OS Recent Advances in Bioinspired Proton-Coupled Electron Transfer. Dalton Trans. 2019, 48, 5861–5868. [PubMed: 30566145]

(12). Milan M; Salamone M; Costas M; Bietti M The Quest for Selectivity in Hydrogen Atom Transfer Based Aliphatic C–H Bond Oxygenation. Acc. Chem. Res 2018, 51, 1984–1995. [PubMed: 30080039]

(13). Davies HML; Manning JR Catalytic C–H Functionalization by Metal Carbenoid and Nitrenoid Insertion. Nature 2008, 451, 417–424. [PubMed: 18216847]

(14). Costas M Remote Oxidation of Aliphatic C–H Bonds with Biologically Inspired Catalysts. In Remote C–H Bond Functionalizations; 2021; pp 383–421.

(15). Rittle J; Green MT Cytochrome P450 Compound I: Capture, Characterization, and C-H Bond Activation Kinetics. Science 2010, 330, 933–937. [PubMed: 21071661]

(16). Mittra K; Green MT Reduction Potentials of P450 Compounds I and II: Insight into the Thermodynamics of C–H Bond Activation. J. Am. Chem. Soc 2019, 141, 5504–5510. [PubMed: 30892878]

(17). Yosca TH; Rittle J; Krest CM; Onderko EL; Silakov A; Calixto JC; Behan RK; Green MT Iron(IV)Hydroxide PKa and the Role of Thiolate Ligation in C–H Bond Activation by Cytochrome P450. Science 2013, 342, 825–829. [PubMed: 24233717]

(18). Shaik S; Kumar D; de Visser SP; Altun A; Thiel W Theoretical Perspective on the Structure and Mechanism of Cytochrome P450 Enzymes. Chem. Rev 2005, 105, 2279–2328. [PubMed: 15941215]

(19). Kaizer J; Klinker EJ; Oh NY; Rohde J-U; Song WJ; Stubna A; Kim J; Münck E; Nam W; Que L Nonheme FeIVO Complexes That Can Oxidize the C–H Bonds of Cyclohexane at Room Temperature. J. Am. Chem. Soc 2004, 126, 472–473. [PubMed: 14719937]

(20). England J; Guo Y; Farquhar ER; Young VG Jr.; Münck E; Que L Jr. The Crystal Structure of a High-Spin Oxoiron(IV) Complex and Characterization of Its Self-Decay Pathway. J. Am. Chem. Soc 2010, 132, 8635–8644. [PubMed: 20568768]

(21). Valdez-Moreira JA; Beagan DM; Yang H; Telser J; Hoffman BM; Pink M; Carta V; Smith JM Hydrocarbon Oxidation by an Exposed, Multiply Bonded Iron(III) Oxo Complex. ACS Cent. Sci 2021, 7, 1751–1755. [PubMed: 34729418]

(22). Panda C; Doyle LM; Gericke R; McDonald AR Rapid Iron(III)–Fluoride-Mediated Hydrogen Atom Transfer. Angew. Chem. Int. Ed 2021, 60, 26281–26286.

(23). Mandal M; Elwell CE; Bouchey CJ; Zerk TJ; Tolman WB; Cramer CJ Mechanisms for Hydrogen-Atom Abstraction by Mononuclear Copper(III) Cores: Hydrogen-Atom Transfer or Concerted Proton-Coupled Electron Transfer? J. Am. Chem. Soc 2019, 141, 17236–17244. [PubMed: 31617707]

(24). Chen MS; White MC A Predictably Selective Aliphatic C–H Oxidation Reaction for Complex Molecule Synthesis. Science 2007, 318, 783–787. [PubMed: 17975062]

(25). Schwarz H; Shaik S; Li J Electronic Effects on Room-Temperature, Gas-Phase C–H Bond Activations by Cluster Oxides and Metal Carbides: The Methane Challenge. J. Am. Chem. Soc 2017, 139, 17201–17212. [PubMed: 29112810]

(26). Baglia RA; Prokop-Prigge KA; Neu HM; Siegler MA; Goldberg DP Mn(V)(O) versus Cr(V)(O) Porphyrinoid Complexes: Structural Characterization and Implications for Basicity Controlling H-Atom Abstraction. J. Am. Chem. Soc 2015, 137, 10874–10877. [PubMed: 26295412]

(27). Groves JT; Takahashi T Activation and Transfer of Nitrogen from a Nitridomanganese(V) Porphyrin Complex. Aza Analog of Epoxidation. J. Am. Chem. Soc 1983, 105, 2073–2074.

(28). Groves JT; Stern MK Synthesis, Characterization, and Reactivity of Oxomanganese(IV) Porphyrin Complexes. J. Am. Chem. Soc 1988, 110, 8628–8638.

(29). Groves JT; Kruper WJ; Haushalter RC Hydrocarbon Oxidations with Oxometalloporphinates. Isolation and Reactions of a (Porphinato)Manganese(V) Complex. J. Am. Chem. Soc 1980, 102, 6375–6377.

(30). Groves JT; Nemo TE Aliphatic Hydroxylation Catalyzed by Iron Porphyrin Complexes. J. Am. Chem. Soc 1983, 105, 6243–6248.

(31). Groves JT; Nemo TE; Myers RS Hydroxylation and Epoxidation Catalyzed by Iron-Porphine Complexes. Oxygen Transfer from Iodosylbenzene. J. Am. Chem. Soc 1979, 101, 1032–1033.

(32). Agarwal RG; Coste SC; Groff BD; Heuer AM; Noh H; Parada GA; Wise CF; Nichols EM; Warren JJ; Mayer JM Free Energies of Proton-Coupled Electron Transfer Reagents and Their Applications. Chem. Rev 2022, 122, 1–49. [PubMed: 34928136]

(33). Barman SK; Jones JR; Sun C; Hill EA; Ziller JW; Borovik AS Regulating the Basicity of Metal–Oxido Complexes with a Single Hydrogen Bond and Its Effect on C–H Bond Cleavage. J. Am. Chem. Soc 2019, 141, 11142–11150. [PubMed: 31274298]

(34). Bell RP; Hinshelwood CN The Theory of Reactions Involving Proton Transfers. Proc. R. Soc. London. Ser. A -Math. Phys. Sci 1936, 154, 414–429.

(35). Evans MG; Polanyi M Inertia and Driving Force of Chemical Reactions. Trans. Faraday Soc 1938, 34, 11–24.

(36). Migliore A; Polizzi NF; Therien MJ; Beratan DN Biochemistry and Theory of Proton-Coupled Electron Transfer. Chem. Rev 2014, 114, 3381–3465. [PubMed: 24684625]

(37). Mayer JM Understanding Hydrogen Atom Transfer: From Bond Strengths to Marcus Theory. Acc. Chem. Res 2011, 44, 36–46. [PubMed: 20977224]

(38). Bryant JR; Mayer JM Oxidation of C–H Bonds by $[(bpy)_2(Py)Ru^{IV}O]^{2+}$ Occurs by Hydrogen Atom Abstraction. J. Am. Chem. Soc 2003, 125, 10351–10361. [PubMed: 12926960]

(39). Warren JJ; Tronic TA; Mayer JM Thermochemistry of Proton-Coupled Electron Transfer Reagents and Its Implications. Chem. Rev 2010, 110, 6961–7001. [PubMed: 20925411]

(40). Usharani D; Lacy DC; Borovik AS; Shaik S Dichotomous Hydrogen Atom Transfer vs Proton-Coupled Electron Transfer During Activation of X–H Bonds (X = C, N, O) by Nonheme Iron–Oxo Complexes of Variable Basicity. J. Am. Chem. Soc 2013, 135, 17090–17104. [PubMed: 24124906]

(41). Bailey WD; Dhar D; Cramblitt AC; Tolman WB Mechanistic Dichotomy in Proton-Coupled Electron-Transfer Reactions of Phenols with a Copper Superoxide Complex. J. Am. Chem. Soc 2019, 141, 5470–5480. [PubMed: 30907590]

(42). Liu T; Tyburski R; Wang S; Fernández-Terán R; Ott S; Hammarström L Elucidating Proton-Coupled Electron Transfer Mechanisms of Metal Hydrides with Free Energy-and Pressure-Dependent Kinetics. J. Am. Chem. Soc 2019, 141, 17245–17259. [PubMed: 31587555]

(43). Huang T; Rountree ES; Traywick AP; Bayoumi M; Dempsey JL Switching between Stepwise and Concerted Proton-Coupled Electron Transfer Pathways in Tungsten Hydride Activation. J. Am. Chem. Soc 2018, 140, 14655–14669. [PubMed: 30362720]

(44). Dongare P; Maji S; Hammarström L Direct Evidence of a Tryptophan Analogue Radical Formed in a Concerted Electron–Proton Transfer Reaction in Water. J. Am. Chem. Soc 2016, 138, 2194–2199. [PubMed: 26871741]

(45). Bronner C; Wenger OS Kinetic Isotope Effects in Reductive Excited-State Quenching of $Ru(2,2'\text{-bipyrazine})_3^{2+}$ by Phenols. J. Phys. Chem. Lett 2012, 3, 70–74.

(46). Bronner C; Wenger OS Proton-Coupled Electron Transfer between 4-Cyanophenol and Photoexcited Rhenium(I) Complexes with Different Protonatable Sites. Inorg. Chem 2012, 51, 8275–8283. [PubMed: 22804105]

(47). Yuasa J; Fukuzumi S Mechanistic Borderline between One-Step Hydrogen Transfer and Sequential Transfers of Electron and Proton in Reactions of NADH Analogues with Triplet Excited States of Tetrazines and $Ru(bpy)_3^{2+*}$. J. Am. Chem. Soc 2006, 128, 14281–14292. [PubMed: 17076501]

(48). Dhar D; Yee GM; Markle TF; Mayer JM; Tolman WB Reactivity of the Copper(III)-Hydroxide Unit with Phenols. Chem. Sci 2017, 8, 1075–1085. [PubMed: 28572905]

(49). Zdilla MJ; Dexheimer JL; Abu-Omar MM Hydrogen Atom Transfer Reactions of Imido Manganese(V) Corrole: One Reaction with Two Mechanistic Pathways. J. Am. Chem. Soc 2007, 129, 11505–11511. [PubMed: 17718564]

(50). Morimoto Y; Park J; Suenobu T; Lee Y-M; Nam W; Fukuzumi S Mechanistic Borderline of One-Step Hydrogen Atom Transfer versus Stepwise Sc^{3+}-Coupled Electron Transfer from Benzyl Alcohol Derivatives to a Non-Heme Iron(IV)-Oxo Complex. Inorg. Chem 2012, 51, 10025–10036. [PubMed: 22954389]

(51). Park J; Morimoto Y; Lee Y-M; Nam W; Fukuzumi S Unified View of Oxidative C–H Bond Cleavage and Sulfoxidation by a Nonheme Iron(IV)–Oxo Complex via Lewis Acid-Promoted Electron Transfer. Inorg. Chem 2014, 53, 3618–3628. [PubMed: 24605985]

(52). Irebo T; Zhang M-T; Markle TF; Scott AM; Hammarström L Spanning Four Mechanistic Regions of Intramolecular Proton-Coupled Electron Transfer in a $Ru(bpy)_3^{2+}$–Tyrosine Complex. J. Am. Chem. Soc 2012, 134, 16247–16254. [PubMed: 22909089]

(53). Zhang M-T; Nilsson J; Hammarström L Bimolecular Proton-Coupled Electron Transfer from Tryptophan with Water as the Proton Acceptor. Energy Environ. Sci 2012, 5, 7732–7736.

(54). Bourrez M; Steinmetz R; Ott S; Gloaguen F; Hammarström L Concerted Proton-Coupled Electron Transfer from a Metal-Hydride Complex. Nat. Chem 2015, 7, 140–145.

(55). Liu T; Guo M; Orthaber A; Lomoth R; Lundberg M; Ott S; Hammarström L Accelerating Proton-Coupled Electron Transfer of Metal Hydrides in Catalyst Model Reactions. Nat. Chem 2018, 10, 881–887. [PubMed: 30013192]

(56). Darcy JW; Kolmar SS; Mayer JM Transition State Asymmetry in C–H Bond Cleavage by Proton-Coupled Electron Transfer. J. Am. Chem. Soc 2019, 141, 10777–10787. [PubMed: 31199137]

(57). Goetz MK; Anderson JS Experimental Evidence for p K a -Driven Asynchronicity in C-H Activation by a Terminal Co(III)-Oxo Complex. J. Am. Chem. Soc 2019, 141, 4051–4062. [PubMed: 30739450]

(58). Elwell CE; Mandal M; Bouchey CJ; Que L; Cramer CJ; Tolman WB Carboxylate Structural Effects on the Properties and Proton-Coupled Electron Transfer Reactivity of $[CuO_2CR]^{2+}$ Cores. Inorg. Chem 2019, 58, 15872–15879. [PubMed: 31710477]

(59). Barman SK; Yang M-Y; Parsell TH; Green MT; Borovik AS Semiempirical Method for Examining Asynchronicity in Metal–Oxido-Mediated C–H Bond Activation. Proc. Natl. Acad. Sci. U.S.A 2021, 118, e2108648118. [PubMed: 34465626]

(60). Schneider JE; Goetz MK; Anderson JS Statistical Analysis of C–H Activation by Oxo Complexes Supports Diverse Thermodynamic Control over Reactivity. Chem. Sci 2021, 12, 4173–4183. [PubMed: 34163690]

(61). Cukier RI; Nocera DG PROTON-COUPLED ELECTRON TRANSFER. Annu. Rev. Phys. Chem 1998, 49, 337–369. [PubMed: 9933908]

(62). Bím D; Maldonado-Domínguez M; Rulíšek L; Srnec M Beyond the Classical Thermodynamic Contributions to Hydrogen Atom Abstraction Reactivity. Proc. Natl. Acad. Sci. U.S.A 2018, 115, E10287–E10294. [PubMed: 30254163]

(63). Tedder JM Which Factors Determine the Reactivity and Regioselectivity of Free Radical Substitution and Addition Reactions? Angew. Chem. Int. Ed 1982, 21, 401–410.

(64). Buckle RN; Liu P-Y; Roberts EWD; Burnell DJ Differences in Rates of Diels-Alder Reactions as Experimental Indicators of Synchronous or Asynchronous Transition States. Tetrahedron 1999, 55, 11455–11464.

(65). Beno BR; Houk KN; Singleton DA Synchronous or Asynchronous? An “Experimental” Transition State from a Direct Comparison of Experimental and Theoretical Kinetic Isotope Effects for a Diels–Alder Reaction. J. Am. Chem. Soc 1996, 118, 9984–9985.

(66). Kotani H; Shimomura H; Ikeda K; Ishizuka T; Shiota Y; Yoshizawa K; Kojima T Mechanistic Insight into Concerted Proton–Electron Transfer of a Ru(IV)-Oxo Complex: A Possible Oxidative Asynchronicity. J. Am. Chem. Soc 2020, 142, 16982–16989. [PubMed: 32924508]

(67). Tyburski R; Liu T; Glover SD; Hammarström L Proton-Coupled Electron Transfer Guidelines, Fair and Square. J. Am. Chem. Soc 2021, 143, 560–576. [PubMed: 33405896]

(68). Costentin C; Savéant J-M Hydrogen and Proton Exchange at Carbon. Imbalanced Transition State and Mechanism Crossover. Chem. Sci 2020, 11, 1006–1010.

(69). Sayfutyarova ER; Lam Y-C; Hammes-Schiffer S Strategies for Enhancing the Rate Constant of C–H Bond Cleavage by Concerted Proton-Coupled Electron Transfer. J. Am. Chem. Soc 2019, 141, 15183–15189. [PubMed: 31464122]

(70). Maldonado-Domínguez M; Bím D; Fučík R; Čurík R; Srnec M Reactive Mode Composition Factor Analysis of Transition States: The Case of Coupled Electron–Proton Transfers. Phys. Chem. Chem. Phys 2019, 21, 24912–24918. [PubMed: 31690920]

(71). Tyburski R; Hammarström L Strategies for Switching the Mechanism of Proton-Coupled Electron Transfer Reactions Illustrated by Mechanistic Zone Diagrams. Chem. Sci 2022, 13, 290–301.

(72). Coste SC; Brezny AC; Koronkiewicz B; Mayer JM C–H Oxidation in Fluorenyl Benzoates Does Not Proceed through a Stepwise Pathway: Revisiting Asynchronous Proton-Coupled Electron Transfer. Chem. Sci 2021, 12, 13127–13136. [PubMed: 34745543]

(73). Sayfutyarova ER; Goldsmith ZK; Hammes-Schiffer S Theoretical Study of C–H Bond Cleavage via Concerted Proton-Coupled Electron Transfer in Fluorenyl-Benzoates. J. Am. Chem. Soc 2018, 140, 15641–15645. [PubMed: 30383371]

(74). Warm K; Paskin A; Kuhlmann U; Bill E; Swart M; Haumann M; Dau H; Hildebrandt P; Ray K A Pseudotetrahedral Terminal Oxoiron(IV) Complex: Mechanistic Promiscuity in C–H Bond Oxidation Reactions. Angew. Chem. Int. Ed 2021, 60, 6752–6756.

(75). Zhang J; Lee Y-M; Seo MS; Kim Y; Lee E; Fukuzumi S; Nam W Oxidative versus Basic Asynchronous Hydrogen Atom Transfer Reactions of Mn(III)-Hydroxo and Mn(Iii)-Aqua Complexes. Inorg. Chem. Front 2022, 9, 3233–3243.

(76). Goetz MK; Hill EA; Filatov AS; Anderson JS Isolation of a Terminal Co(III)-Oxo Complex. J. Am. Chem. Soc 2018, 140, 13176–13180. [PubMed: 30078327]

(77). Goetz MK; Schneider JE; Filatov AS; Jesse KA; Anderson JS Enzyme-Like Hydroxylation of Aliphatic C–H Bonds From an Isolable Co-Oxo Complex. J. Am. Chem. Soc 2021, 143, 20849–20862. [PubMed: 34856101]

(78). Schäfer A; Horn H; Ahlrichs R Fully Optimized Contracted Gaussian Basis Sets for Atoms Li to Kr. J. Chem. Phys 1992, 97, 2571–2577.

(79). Schäfer A; Huber C; Ahlrichs R Fully Optimized Contracted Gaussian Basis Sets of Triple Zeta Valence Quality for Atoms Li to Kr. J. Chem. Phys 1994, 100, 5829–5835.

(80). Weigend F; Ahlrichs R Balanced Basis Sets of Split Valence, Triple Zeta Valence and Quadruple Zeta Valence Quality for H to Rn: Design and Assessment of Accuracy. Phys. Chem. Chem. Phys 2005, 7, 3297–3305. [PubMed: 16240044]

(81). Yu-Ran Luo. Handbook of Bond Dissociation Energies in Organic Compounds; CRC Press, 2003.

(82). HANDY NC; COHEN AJ Left-Right Correlation Energy. Mol. Phys 2001, 99, 403–412.

(83). COHEN AJ; HANDY NC Dynamic Correlation. Mol. Phys 2001, 99, 607–615.

(84). Hansch C; Leo A; Taft RW A Survey of Hammett Substituent Constants and Resonance and Field Parameters. Chem. Rev 1991, 91, 165–195.

(85). Lansky DE; Goldberg DP Hydrogen Atom Abstraction by a High-Valent Manganese(V)–Oxo Corrolazine. Inorg. Chem 2006, 45, 5119–5125. [PubMed: 16780334]

(86). Rochester CH; Rossall B Steric Hindrance and Acidity. Part 3.—Enthalpies and Entropies of Ionization of Phenols in Methanol. Trans. Faraday Soc 1969, 65, 1004–1013.

(87). Bordwell FG; Zhang X-M Acidities and Homolytic Bond Dissociation Enthalpies of 4-Substituted-2,6-Di-Tert-Butylphenols. J. Phys. Org. Chem 1995, 8, 529–535.

(88). Schneider J; Goetz MK; Anderson J Reconciling Imbalanced Transition State Effects with Nonadiabatic CPET Reactions. ChemRxiv DOI: 10.33774/chemrxiv-2021-xp9mj.

(89). Parsell TH; Behan RK; Green MT; Hendrich MP; Borovik AS Preparation and Properties of a Monomeric MnIV–Oxo Complex. J. Am. Chem. Soc 2006, 128, 8728–8729. [PubMed: 16819856]

(90). Kotani H; Kaida S; Ishizuka T; Sakaguchi M; Ogura T; Shiota Y; Yoshizawa K; Kojima T Formation and Characterization of a Reactive Chromium(V)–Oxo Complex: Mechanistic Insight into Hydrogen-Atom Transfer Reactions. Chem. Sci 2015, 6, 945–955. [PubMed: 29560181]

(91). Zheng H-X; Xiao Z-F; Yao C-Z; Li Q-Q; Ning X-S; Kang Y-B; Tang Y Transition-Metal-Free Self-Hydrogen-Transferring Allylic Isomerization. Org. Lett 2015, 17, 6102–6105. [PubMed: 26618248]

(92). Neese F The ORCA Program System. Wiley Interdiscip. Rev. Comput. Mol. Sci 2012, 2, 73–78.

(93). Neese F; Wennmohs F; Hansen A; Becker U Efficient, Approximate and Parallel Hartree–Fock and Hybrid DFT Calculations. A ‘Chain-of-Spheres’ Algorithm for the Hartree–Fock Exchange. Chem. Phys 2009, 356, 98–109.

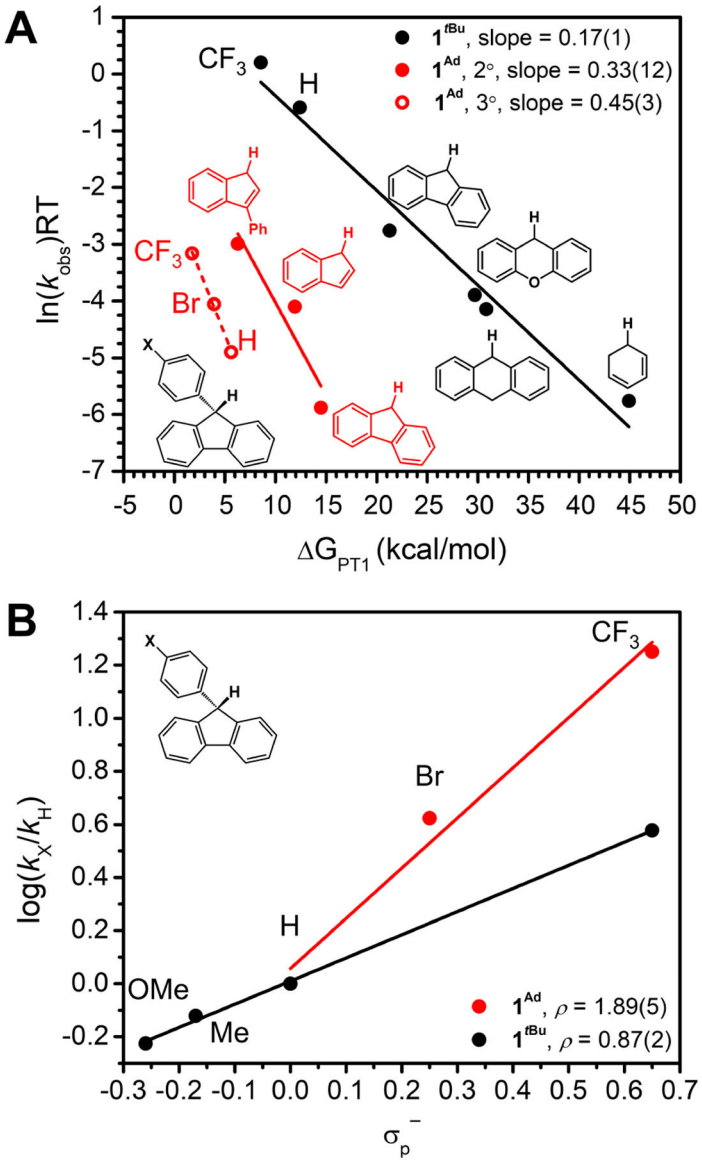

Figure 1.

(A) Plot of ln(k_{obs})RT versus ΔG_{PT1} for **1^{tBu}** and **1^{Ad}** reacting with various C–H substrates. ΔG_{PT1} was calculated by DFT. R^2 = **1^{tBu}**: 0.96, **1^{Ad}**, 2° substrates: 0.77, **1^{Ad}**, 3° substrates: 0.99. (B) Hammett analyses for the reaction of **1^{tBu}** and **1^{Ad}** with *p*-substituted 9-phenylfluorenes. The red dot for X = H for **1^{Ad}** is hidden under the black dot for **1^{tBu}**. Solid lines indicate linear fits to the data. R^2 = **1^{tBu}**: >0.99, **1^{Ad}**: 0.97. All reactions with **1^{tBu}** were carried out with 10 equiv. substrate and the data is from Ref. 57. Reactions with **1^{Ad}** were carried out with 50 equiv. substrate, k_{obs} values were divided by 5 for the plot in (A).

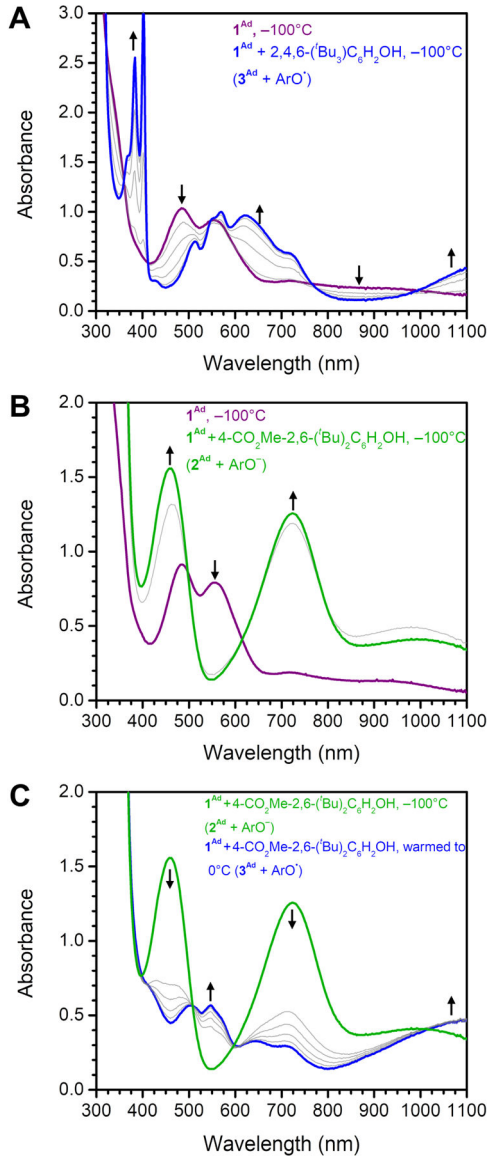

Figure 2.

UV-vis traces of phenol substrates with **1**$^{\mathbf{Ad}}$ in THF. A) 2,4,6-(*t*Bu)$_3$C$_6$H$_2$OH at −100 °C showing a concerted mechanism. B) 4-CO$_2$Me-2,6-(*t*Bu)$_2$C$_6$H$_2$OH at −100°C showing only PT. C) Warming of B) to 0 °C showing ET. Gray traces show intermediate time point spectra.

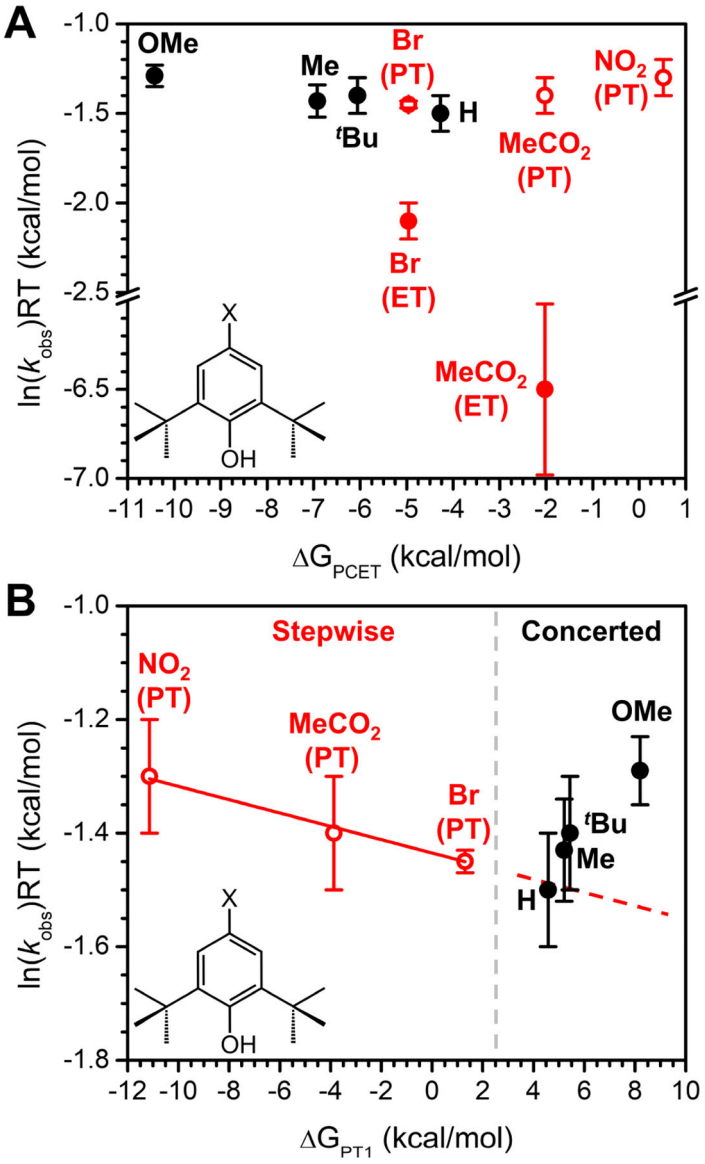

Figure 3.

ln(k_{obs})RT for the reaction between **1**^{Ad} and 10 equiv. of a substituted phenol plotted vs. A) the free energies for CPET and B) the free energies for PT1. In A) The Y-axis has a break from −2.5 to −6. Error bars indicate the standard error of the mean from multiple trials. Solid red circles indicate PT rates, hollow red circles indicate ET rates, and solid black spheres indicate PCET rates, as determined from UV-vis analysis as discussed and shown in Figure 2. In B) the gray dashed line delineates a crossover between stepwise and concerted reactivity and the red dashed line shows an extrapolation of the expected ln(k_{obs})RT values if were able to observe *only* PT for all substrates, illustrating the maximum expected ln(k_{obs})RT values for stepwise PTET mechanisms (see discussion in SI). The k_{obs} values used to determine ln(k_{obs})RT for the stepwise (red) substrates are for PT1 to generate **2**^{Ad} and the corresponding phenoxide and the k_{obs} values used to determine ln(k_{obs})RT for the

concerted (black) substrates are for CPET to generate $\mathbf{3}^{\mathbf{Ad}}$ and the corresponding phenoxyl radical.

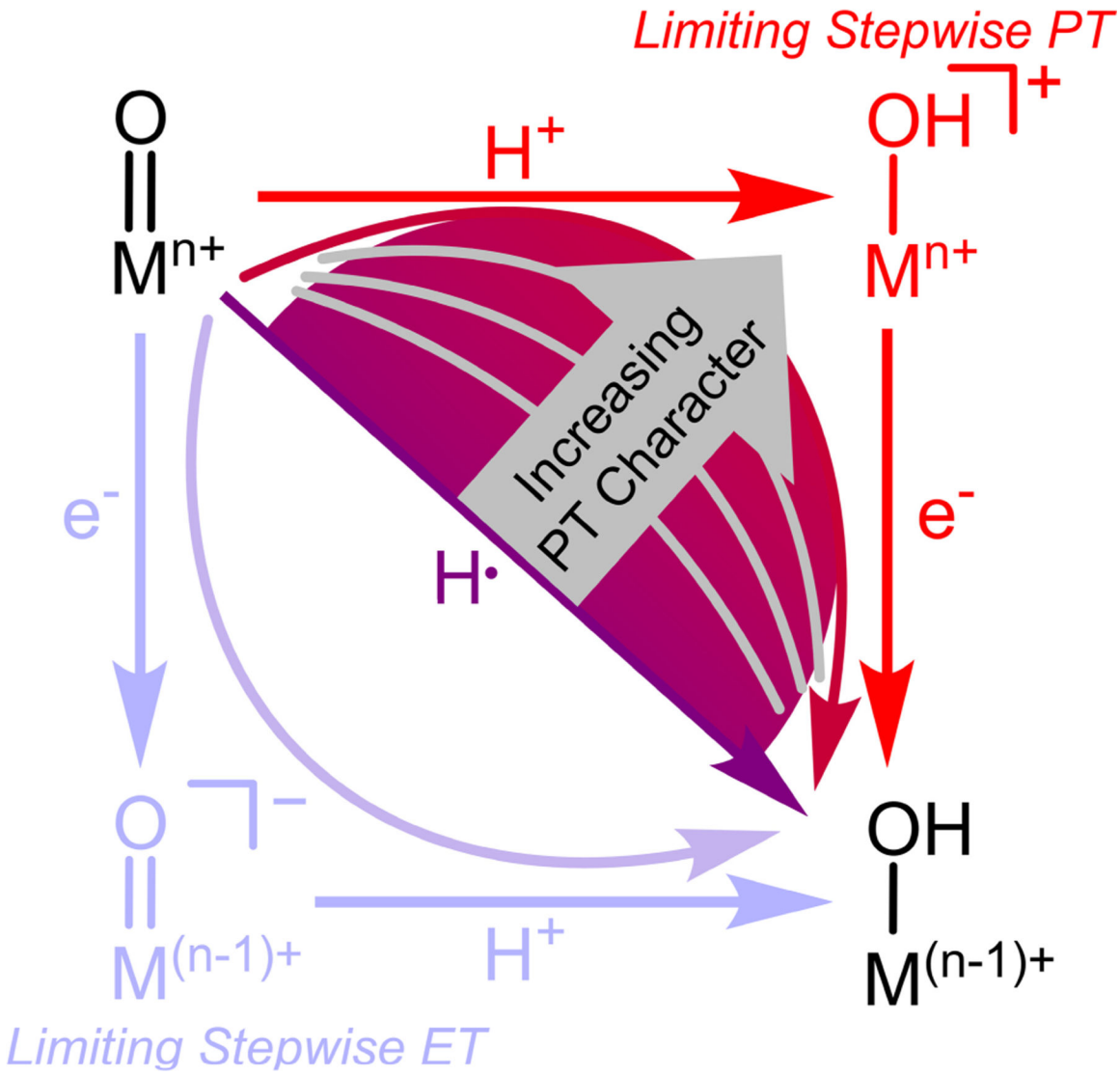

Scheme 1.
Square scheme depicting limiting stepwise pathways and PT-dependent CPET pathways.

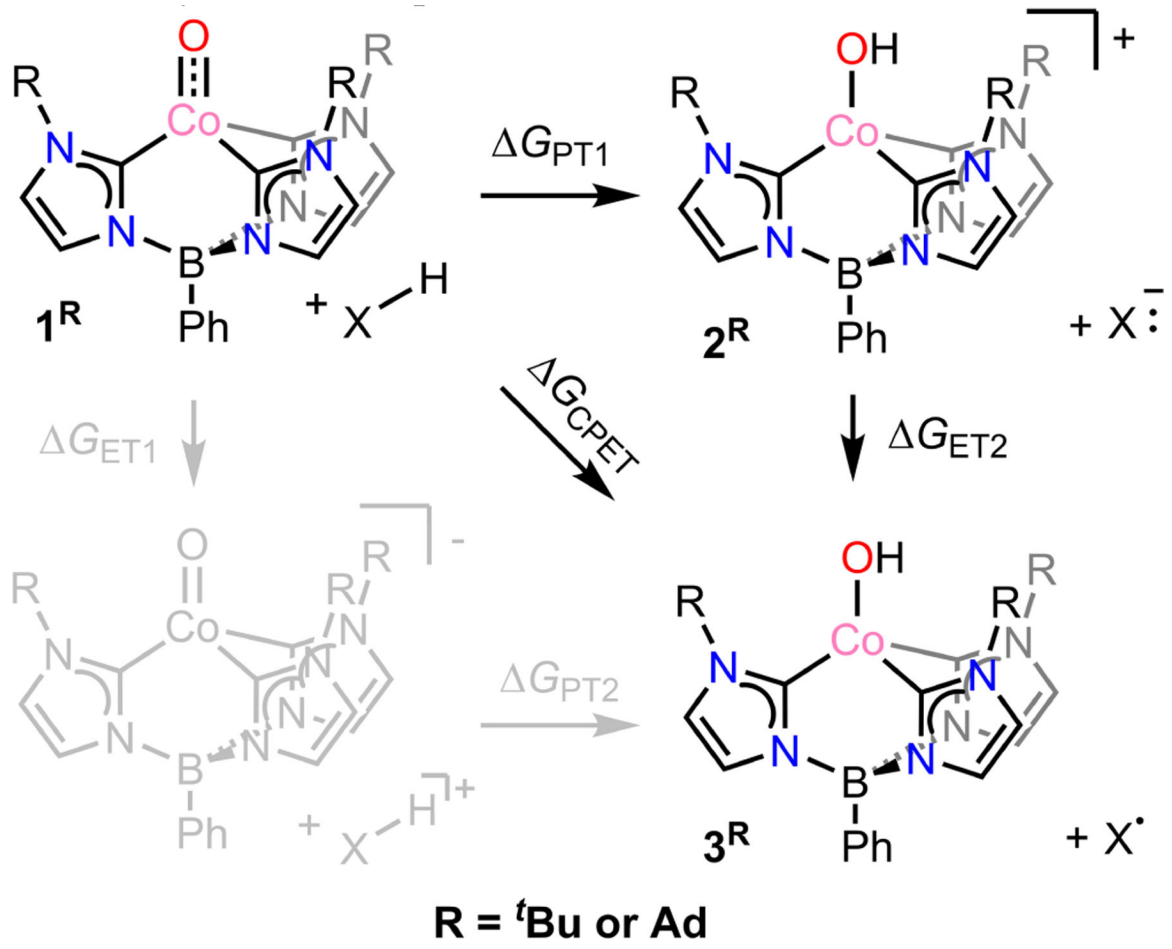

Scheme 2.
Co complexes discussed in this work and possible elementary reaction steps.

Table 1.

Thermodynamic and Kinetic Data for the Reaction of $\mathbf{1^{Ad}}$ with 4-X-2,6-di(*tert*-butyl)phenols.

X	ΔG_{CPET}	ΔG_{PTI}	η	$\ln(k_{obs})RT$[a]
OMe	−10.42	8.20	−52.3	−1.29(6)
Me	−6.92	5.21	−59.2	−1.43(9)
^{t}Bu	−6.06	5.44	−60.1	−1.4(1)
H	−4.27	4.58	−64.1	−1.5(1)
Br	−4.96	1.30	−65.4	−1.45(2) (PT) −2.1(1) (ET)
CO_2Me	−2.03	−3.87	−74.8	−1.4(1) (PT) −6.5(5) (ET)
NO_2	0.52	−11.14	−85.1	−1.3(1) (PT)

Units for all values in kcal/mol.

[a]CPET reaction between $\mathbf{1^{Ad}}$ and 10 equivalents of phenol substrate at −100 °C unless otherwise noted. Stepwise substrates (X = Br, CO_2Me, and NO_2) have both the $\ln(k_{obs})RT$ values for initial PT (with the same conditions as the concerted substrates) as well as the $\ln(k_{obs})RT$ values for ET (reaction between $\mathbf{2^{Ad}}$ and 10 equivalents of phenolate, extrapolated to −100 °C with an Arrhenius analysis) reported. Note that the k_{obs} for ET for X = NO_2 was not determined.